

Cite this: *Chem. Commun.*, 2012, **48**, 9150–9152

www.rsc.org/chemcomm

## COMMUNICATION

**Block copolymer assisted synthesis of porous  $\alpha$ -Ni(OH)<sub>2</sub> microflowers with high surface areas as electrochemical pseudocapacitor materials†**Bishnu Prasad Bastakoti,<sup>a</sup> Hou-Sheng Huang,<sup>b</sup> Lin-Chi Chen,<sup>\*b</sup> Kevin C.-W. Wu<sup>\*c</sup> and Yusuke Yamauchi<sup>\*ade</sup>

Received 25th April 2012, Accepted 18th July 2012

DOI: 10.1039/c2cc32945j

**Porous  $\alpha$ -Ni(OH)<sub>2</sub> microflowers are successfully synthesized via a one-step aqueous-phase reaction assisted by block copolymers under mild conditions. The electrochemical measurement demonstrates that the  $\alpha$ -Ni(OH)<sub>2</sub> microflowers calcined at 200 °C are capable to deliver a specific capacity of 1551 F g<sup>-1</sup> in 6 M KOH solution, suggesting their high potential as a novel electrochemical pseudocapacitor.**

Supercapacitors have attracted considerable attention in recent years, because they offer extremely high power density, long cycle life, short charging time, and minimal safety concerns.<sup>1</sup> Various materials such as transition metal oxides (*e.g.*, RuO<sub>2</sub>) have been extensively investigated for possible applications as supercapacitors.<sup>2</sup> However, those materials are not suitable for industrial applications due to very high cost. Considerable effort is being devoted to developing “inexpensive” electrode materials.

Ni(OH)<sub>2</sub> is a promising alternative electrode material due to its low cost, high theoretical specific capacitance, well-defined electrochemical redox activity, easy availability and high stability in alkaline electrolytes.<sup>3</sup> To date, numerous works have been developed to synthesize Ni(OH)<sub>2</sub> with different morphologies, because the electrochemical performances of Ni(OH)<sub>2</sub> are directly affected by its morphology and particle size.<sup>4</sup> Tao *et al.* synthesized Ni(OH)<sub>2</sub> microtubes by a template-free wet-chemical method.<sup>5</sup> Microrods, microplates, microspheres of Ni(OH)<sub>2</sub> have been also synthesized and their electrochemical properties have been studied.<sup>6</sup> Among the several morphologies, flower-shaped

Ni(OH)<sub>2</sub> microstructures have attracted considerable attention, because of short diffusion path lengths for both electrolyte ions and electrons, favouring high diffusion and easy migration of electrolyte ions during the rapid charge–discharge process.<sup>7</sup>

Most of the previous works on Ni(OH)<sub>2</sub> are on  $\beta$ -Ni(OH)<sub>2</sub>.<sup>8</sup> Ni(OH)<sub>2</sub> has two polymorphs;  $\alpha$ - and  $\beta$ -Ni(OH)<sub>2</sub>. The  $\alpha$ -phase contains stacked and positively-charged Ni(OH)<sub>2</sub> layers with exchangeable anions and water molecules intercalated into the interlayer space to balance the positive charges. The  $\beta$ -phase structurally consists of an ordered stacking of well-oriented Ni(OH)<sub>2</sub> layers without any intercalated species.<sup>9</sup> In general,  $\alpha$ -Ni(OH)<sub>2</sub> shows better electrochemical properties than  $\beta$ -Ni(OH)<sub>2</sub>. However, the  $\alpha$ -Ni(OH)<sub>2</sub> phase is hard to prepare due to its easy phase transformation into the  $\beta$ -Ni(OH)<sub>2</sub> phase.<sup>10</sup>

Here, we demonstrate a simple, cost-effective, and solution-based approach for the synthesis of  $\alpha$ -Ni(OH)<sub>2</sub> microflowers with the assistance of a commercially available triblock copolymer (F127) (Fig. 1). The obtained  $\alpha$ -Ni(OH)<sub>2</sub> microflowers consist of assembled nanosheets in random directions. The as-prepared  $\alpha$ -Ni(OH)<sub>2</sub> microflowers were then calcined at different temperatures to tune the crystal phases, crystallinity, and surface areas (Fig. S1, ESI†), which would affect their electrochemical performance.

In this experimental work,  $\alpha$ -Ni(OH)<sub>2</sub> microflowers were prepared by mixing Ni(NO<sub>3</sub>)<sub>2</sub>, F127, and urea. F127 works as a sort of structure directing agent, whereas the urea is a precipitating agent. The slow hydrolysis of urea upon heating causes precipitation of Ni(OH)<sub>2</sub>. The slow hydrolysis of urea releases ammonia. The ammonia can form a complex [Ni(NH<sub>3</sub>)<sub>x</sub><sup>2+</sup>] with Ni<sup>2+</sup>. The coordinated NH<sub>3</sub> molecules interact with polyethylene oxide chains (PEO) of F127 units through hydrogen bonding, which is a driving force for the interaction of metal ions with the polymer.<sup>11</sup>

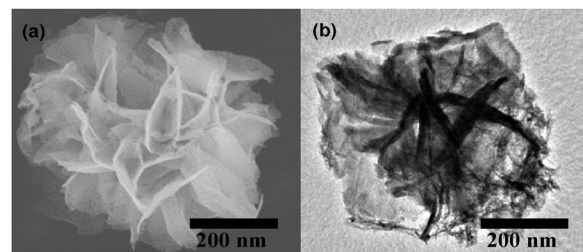


**Fig. 1** (a) SEM image and (b) TEM image of porous  $\alpha$ -Ni(OH)<sub>2</sub> microflowers calcined at 200 °C.

<sup>a</sup> World Premier International (WPI) Research Center for Materials Nanoarchitectonics (MANA), National Institute for Materials Science (NIMS), 1-1 Namiki, Tsukuba, Ibaraki 305-0044, Japan. E-mail: Yamauchi.Yusuke@nims.go.jp

<sup>b</sup> Department of Bio-Industrial Mechatronics Engineering, National Taiwan University, No. 1, Sec. 4, Roosevelt Road, Taipei 10617, Taiwan. E-mail: chenlinchi@ntu.edu.tw

<sup>c</sup> Department of Chemical Engineering, National Taiwan University, No. 1, Sec. 4, Roosevelt Road, Taipei 10617, Taiwan. E-mail: kevinwu@ntu.edu.tw

<sup>d</sup> PRESTO, Japan Science and Technology Agency (JST), Saitama, Japan

<sup>e</sup> Faculty of Science and Engineering, Waseda University, 3-4-1 Okubo, Shinjuku, Tokyo 169-8555, Japan

† Electronic supplementary information (ESI) available: Details of the experimental procedure, SEM images, TG-DTA curves, N<sub>2</sub> adsorption isotherms of the samples at various temperatures. See DOI: 10.1039/c2cc32945j

Yuan *et al.* synthesized Ni(OH)<sub>2</sub> microparticles *via* amino-based complex metal ions. The combination of NH<sub>3</sub> with Ni<sup>2+</sup> ions decreases free Ni<sup>2+</sup> ions concentration, which ultimately reduces the rate of unnecessary crystal growth.<sup>12</sup>

The concentration of the F127 surfactant is very important to tune the morphology of microstructures. When the concentration of the polymer was decreased up to 0.1 g L<sup>-1</sup>, several irregular structures appeared (Fig. S2a, ESI†). In this case, the polymer amount was not enough to direct the flower-shaped  $\alpha$ -Ni(OH)<sub>2</sub> structure. In contrast, when the concentration of the polymer became very high (30 g L<sup>-1</sup>), the flower-like structure was observed. But, several particles were aggregated with each other (Fig. S2b, ESI†). At high concentration, the polymer forms multicellular aggregates due to intermicellar association,<sup>13</sup> which might hinder good dispersion of the particles. Thus, the F127 concentration is a critical factor to achieve the well-developed flower-shaped structures. Hereafter, we fix the F127 concentration at 5 g L<sup>-1</sup> throughout the study.

Fig. 2a shows wide-angle XRD profiles of as-prepared and calcined samples. The peaks of the as-prepared sample were assignable to  $\alpha$ -Ni(OH)<sub>2</sub> (JCPDS No:38-0715).<sup>14</sup> The sharp diffraction peaks confirmed the high crystallinity of the as-prepared material. The average crystallite size estimated by the Scherrer equation from the (003) peak was around 4 nm. No peaks of any other impurities were detected, suggesting high purity of the turbostratic phase of  $\alpha$ -Ni(OH)<sub>2</sub>. In order to tune the crystalline phases and crystallinities, the as-prepared sample was calcined at different temperatures. The crystalline phase of  $\alpha$ -Ni(OH)<sub>2</sub> was retained until the temperature was increased to 200 °C. Calcination at higher temperature ( $\geq 300$  °C) induced transformation from  $\alpha$ -Ni(OH)<sub>2</sub> to NiO, as confirmed by XRD profiles in Fig. 2a. The peaks derived from  $\alpha$ -Ni(OH)<sub>2</sub> completely disappeared and new peaks (111, 200, 220, and 311) appeared, which are all consistent with the face-centered cubic

(*fcc*) NiO phase (JCPDS No.47-1049). It has been generally known that the decomposition of  $\alpha$ -Ni(OH)<sub>2</sub> into NiO completes at around 300 °C,<sup>15</sup> which coincided with the present study. The thermal decomposition of Ni(OH)<sub>2</sub> took place at a lower temperature than 300 °C,<sup>16</sup> but the transformation of Ni(OH)<sub>2</sub> into NiO was not complete at such a low temperature. For example, for the  $\alpha$ -Ni(OH)<sub>2</sub> microflowers calcined at 200 °C, a very small (111) peak derived from the NiO phase was also observed. With further increase of the calcination temperature (from 300 to 600 °C), the FWHM (full width at half maximum) of each peak decreased, indicating that the crystal grains of NiO became larger. From SEM observation (Fig. S1, ESI†), it was proved that the original flower morphology of the as-prepared material was retained till the calcined temperature reaches 400 °C. When the calcination temperature was further increased, the flower morphology gradually disappeared, indicating that the NiO nanosheets were not stable at high temperatures.

The phase transformation of  $\alpha$ -Ni(OH)<sub>2</sub> to NiO was also examined by TG-DTA analysis. The initial slope on the TG curves (Fig. S3, ESI†) was desorption of physically-absorbed and/or structurally-bonded water molecules. The endothermic peak centered at around 205 °C is due to the combustion of the block copolymer. Whereas the endothermic peak around 300 °C can be assigned to the phase transformation of  $\alpha$ -Ni(OH)<sub>2</sub> into NiO by loss of water produced by dehydroxylation of hydroxide sheets, which was also confirmed by XRD measurement (Fig. 2a).

The BET surface areas of all the samples were characterized by N<sub>2</sub> adsorption–desorption isotherms. The surface areas of all the samples calcined at different temperatures are shown in Fig. S1 and S4 (ESI†). When the calcination temperatures were higher than 300 °C, the crystal grains of the nickel oxides grew (as observed in Fig. 2a) and the pore networks shrunk, thereby seriously decreasing the surface areas (inset of Fig. S1, ESI†). The high magnification SEM and TEM images of the  $\alpha$ -Ni(OH)<sub>2</sub> microflowers calcined at 200 °C (with the highest surface area among other  $\alpha$ -Ni(OH)<sub>2</sub> samples) are shown in Fig. 1. The thin Ni(OH)<sub>2</sub> nanosheets were strongly interconnected to form flower-like structure. Raman spectroscopy was also performed to obtain further information on the sample. The characteristics peaks at 452 cm<sup>-1</sup> and 1040 cm<sup>-1</sup> in Fig. 2b confirmed the  $\alpha$ -Ni(OH)<sub>2</sub> formation.<sup>17</sup>

We evaluated the electrochemical performance of the synthesized materials as pseudocapacitors (Fig. 3). Typical CV curves of  $\alpha$ -Ni(OH)<sub>2</sub> microflowers (calcined at 200 °C) consisted of a pair of strong redox peaks, as shown in Fig. 3a. One peak is anodic during the oxidation reaction of Ni<sup>2+</sup> to Ni<sup>3+</sup>, and the other is cathodic during the reverse process, indicating that the capacitance characteristics are mainly supplied by the faradaic reaction  $\alpha$ -Ni(OH)<sub>2</sub> + OH<sup>-</sup>  $\leftrightarrow$   $\gamma$ -NiOOH + H<sub>2</sub>O + e<sup>-</sup>.<sup>18</sup>

Such a peak potential difference can be regarded as quasi-reversible. The shape of the CV curves was basically constant even at high scan rates (not shown), which resulted from the improved mass transportation within the electrode material.<sup>19</sup>

For example, our  $\alpha$ -Ni(OH)<sub>2</sub> microflowers (calcined at 200 °C) were enabled to deliver a specific capacity of 469 F g<sup>-1</sup> and 229 F g<sup>-1</sup> at the scan rate of 5 mV s<sup>-1</sup> and 25 mV s<sup>-1</sup> in 1 M KOH solution, respectively. The capacitance decreased while the scan rate increased, which can be attributed to more

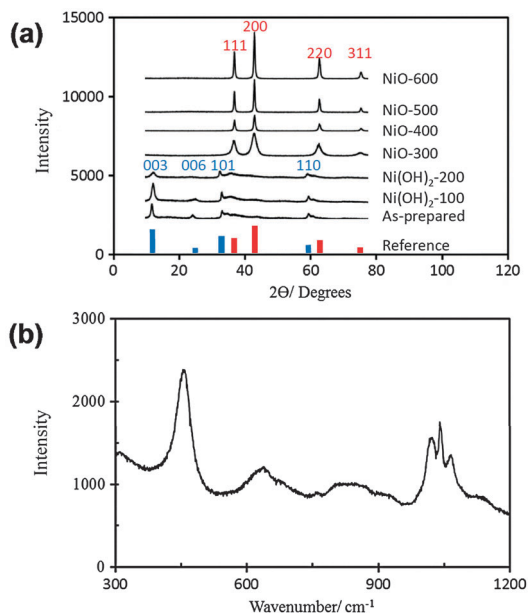


**Fig. 2** (a) XRD patterns of the samples calcined at different temperatures. In the reference, blue-coloured peaks indicate the  $\alpha$ -Ni(OH)<sub>2</sub> phase, while red-coloured peaks indicate the NiO phase. (b) Raman spectra of porous  $\alpha$ -Ni(OH)<sub>2</sub> microflowers calcined at 200 °C.

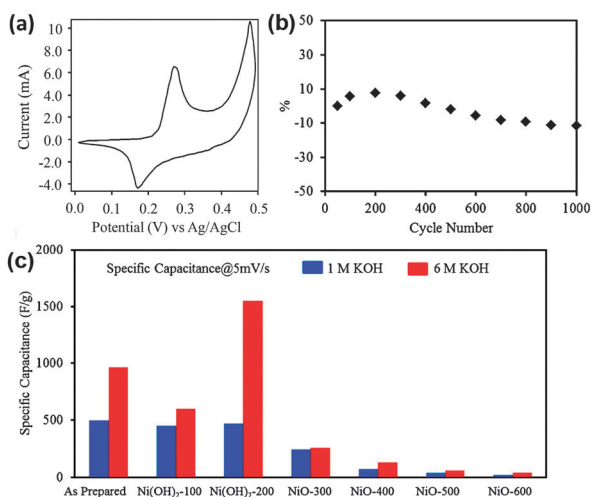


**Fig. 3** (a) CV curve of porous  $\alpha$ -Ni(OH)<sub>2</sub> microflowers calcined at 200 °C (6 M KOH). Scan rate is 5 mV s<sup>-1</sup>. (b) Capacitance retention (%) versus the cycle number of porous  $\alpha$ -Ni(OH)<sub>2</sub> microflowers calcined at 200 °C. (c) Summary of specific capacitance values of the samples calcined at different temperatures. Two different electrolytes (1 M KOH and 6 M KOH) are compared.

difficult penetration and diffusion of the electrolyte (*i.e.*, some parts of the electrode surface become inaccessible) at high scan rates.<sup>20</sup> We also examined the capacitance in 6 M KOH. Commonly, 6 M KOH has been selected as the electrolyte, because the high ion concentration can enhance the conductivity of the electrolyte.<sup>21</sup> The capacitance values for all the samples are shown in Fig. 3c. The maximum capacitance value was observed to be 1551 F g<sup>-1</sup> for the  $\alpha$ -Ni(OH)<sub>2</sub> sample (*i.e.*, calcination temp.: 200 °C, scan rate: 5 mV s<sup>-1</sup>, electrolyte: 6 M KOH), as calculated from the CV curve shown in Fig. 3a. The high capacitance value was supposed to be resulted from the structurally bonded water on the sample.<sup>24</sup> Comparison of our data with various published data on NiO/Ni(OH)<sub>2</sub>-based supercapacitors is summarized in Table S1 (ESI<sup>†</sup>). Long-term cycling stability of electrode material is a critical requirement for practical application (Fig. 3b). Our 200 °C-calcined Ni(OH)<sub>2</sub> micro-flowers showed excellent cycle stability. The capacitance retention slightly increased to 7% after the first 200 cycles, instead of decreasing as in the most cycling stability test in the previous literature.<sup>23</sup> The capacitance loss after 1000 cycles was only 10%.

When the as-prepared samples were calcined over 300 °C, their capacitances greatly decreased, as shown in Fig. 3c. The XRD results in Fig. 2a indicated that the 300 °C-calcined sample was no longer in the  $\alpha$ -Ni(OH)<sub>2</sub> phase and it transformed into the NiO phase. In addition, the CV curve of the NiO phase was very different from that of  $\alpha$ -Ni(OH)<sub>2</sub>. For example, unlike the  $\alpha$ -Ni(OH)<sub>2</sub> phase exhibiting a couple of redox peaks in its CV curve, the NiO phase showed almost no redox peaks in the CV curve. This is because the NiO phase was inert to the electrolyte and its faradaic reaction was unlikely to occur.<sup>16,22</sup> The different electrochemical CV behavior indicated that the capacitance characteristics are mainly supplied by the faradaic reaction of  $\alpha$ -Ni(OH)<sub>2</sub> and by the electrical double layer of NiO. After the NiO phase was formed, further increase of the calcination temperature caused the increase in the crystal sizes (Fig. 2a) and

accordingly decreased the surface area (inset of Fig. S1, ESI<sup>†</sup>), thereby seriously decreasing the capacitance (Fig. 3c).<sup>25</sup>

In conclusion, we successfully synthesized well-defined porous  $\alpha$ -Ni(OH)<sub>2</sub> microflowers by using commercial block copolymers (F127) followed by controlled heat treatment. The finding is very encouraging in view of easy synthetic routes and our material would be a very promising electrode material for future pseudocapacitors.

## Notes and references

- (a) G. Wang, L. Zhang and J. Zhang, *Chem. Soc. Rev.*, 2012, **41**, 797; (b) J. R. Miller and P. Simon, *Science*, 2008, **321**, 651; (c) P. Simon and Y. Gogotsi, *Nat. Mater.*, 2008, **7**, 845.
- (a) L. L. Zhang and X. S. Zhao, *Chem. Soc. Rev.*, 2009, **38**, 2520; (b) R. Vellacheri, V. K. Pillai and S. Kurungot, *Nanoscale*, 2012, **4**, 890.
- (a) H. Wang, H. S. Casalongue, Y. Liang and H. Dai, *J. Am. Chem. Soc.*, 2010, **132**, 7472; (b) H. Jiang, T. Zhao, C. Li and J. Ma, *J. Mater. Chem.*, 2011, **21**, 3818; (c) S. Ida, D. Shiga, M. Koinuma and Y. Matsumoto, *J. Am. Chem. Soc.*, 2008, **130**, 14038; (d) Z. Tang, C. Tang and H. Gong, *Adv. Funct. Mater.*, 2012, **22**, 1272.
- (a) Y. Li, B. Tan and Y. Wu, *Chem. Mater.*, 2008, **20**, 567; (b) D. Wang, C. Song, Z. Hu and X. Fu, *J. Phys. Chem. B*, 2005, **109**, 1125; (c) B. Li, M. Ai and Z. Xu, *Chem. Commun.*, 2010, **46**, 6267.
- F. Tao, M. Guan, Y. Zhou, L. Zhang, Z. Xu and J. Chen, *Cryst. Growth Des.*, 2008, **8**, 2157.
- D. Wang, C. Song, Z. Hu and X. Fu, *J. Phys. Chem. B*, 2005, **109**, 1125.
- J. Yan, Z. Fan, W. Sun, G. Ning, T. Wei, Q. Zhang, R. Zhang, L. Zhi and F. Wei, *Adv. Funct. Mater.*, 2012, **22**, 2632.
- (a) F. Cai, G. Y. Zhang, J. Chen, X. L. Gou, H. K. Liu and S. X. Dou, *Angew. Chem., Int. Ed.*, 2004, **43**, 4212; (b) Y. Qi, H. Qi, C. Lu, Y. Yang and Y. Zhao, *J. Mater. Sci.: Mater. Electron.*, 2009, **20**, 479; (c) S. Zhang and H. C. Zeng, *Chem. Mater.*, 2009, **21**, 871.
- (a) C. Faure, C. Delmas and P. Willmann, *J. Power Sources*, 1991, **36**, 497; (b) Y. Luo, G. Li, G. Duan and L. Zhang, *Nanotechnology*, 2006, **17**, 4278.
- (a) B. Mavis and M. Akinc, *J. Power Sources*, 2004, **134**, 30817; (b) Y. Ren and L. Gao, *J. Am. Ceram. Soc.*, 2010, **93**, 3560.
- A. F. Demirors, B. E. Eser and O. Dag, *Langmuir*, 2005, **21**, 4156.
- C. Yuan, X. Zhang, L. Su, B. Gao and Laifa Shen, *J. Mater. Chem.*, 2009, **19**, 5772.
- (a) S. Guragain, B. P. Bastakoti, S. Yusa and K. Nakashima, *Polymer*, 2010, **51**, 3181; (b) I. W. Hamley, *The physics of block copolymers*, Oxford University Press, New York, USA, 1998.
- (a) S. Shang, K. Xue, D. Chen and X. Jiao, *CrystEngComm*, 2011, **13**, 5094; (b) S. Yang, X. Wu, C. Chen, H. Dong, W. Hu and X. Wang, *Chem. Commun.*, 2012, **48**, 2773.
- (a) B. Zhao, X. K. Ke, J. H. Bao, C. L. Wang, L. Dong, Y. W. Chen and H. L. Chen, *J. Phys. Chem. C*, 2009, **113**, 14440; (b) N. D. Hoa and S. A. El-Safy, *Chem.-Eur. J.*, 2011, **17**, 12896; (c) H. W. Ha, T. W. Kim, J. H. Choy and S. J. Hwang, *J. Phys. Chem. C*, 2009, **113**, 21941.
- J. W. Lang, L. B. Kong, W. J. Wu, Y. C. Luo and L. Kang, *Chem. Commun.*, 2008, 4213.
- (a) C. Johnston and P. R. Gaves, *Appl. Spectrosc.*, 1990, **44**, 105; (b) M. C. Bernard, P. Bernard, M. Keddad, S. Senyariich and H. Takenouti, *Electrochim. Acta*, 1996, **41**, 91.
- S. Yang, X. Wu, C. Chen, H. Dong, W. Hu and X. Wang, *Chem. Commun.*, 2012, **48**, 2773.
- J. Yan, W. Sun, T. Wei, Q. Zhang, Z. Fan and F. Wei, *J. Mater. Chem.*, 2012, **22**, 11494.
- R. R. Salunkhe, K. Jang, S. Lee and H. Ahn, *RSC Adv.*, 2012, **2**, 3190.
- L. Xiao, J. T. Lu, P. F. Liu, L. Zhuang, J. Yan, Y. Hu, B. Mao and C. Lin, *J. Phys. Chem. B*, 2005, **109**, 3860.
- M. Ramani, B. S. Haran, R. E. White and B. N. Popov, *J. Electrochem. Soc.*, 2001, **148**, 374.
- (a) C. C. Hu, K. H. Chang and T. Y. Hsu, *J. Electrochem. Soc.*, 2008, **155**, 196; (b) C. Z. Yuan, X. G. Zhang, L. H. Su, B. Gao and L. F. Shen, *J. Mater. Chem.*, 2009, **19**, 5772.
- V. Ganesh and V. Lakshminarayanan, *Electrochim. Acta*, 2004, **49**, 3561.
- A. Katagiri and M. Nakata, *J. Electrochem. Soc.*, 2003, **150**, C585.